

UC Irvine

UC Irvine Previously Published Works

Title

Interpreting Ionic Conductivity for Polymer Electrolyte Fuel Cell Catalyst Layers with Electrochemical Impedance Spectroscopy and Transmission Line Modeling

Permalink

<https://escholarship.org/uc/item/7mb5r9dw>

Journal

Journal of The Electrochemical Society, 168(5)

ISSN

0013-4651

Authors

Qi, Yongzhen
Liu, Jiangjin
Sabarirajan, Dinesh C
et al.

Publication Date

2021-05-01

DOI

10.1149/1945-7111/abf96d

Peer reviewed

OPEN ACCESS

Interpreting Ionic Conductivity for Polymer Electrolyte Fuel Cell Catalyst Layers with Electrochemical Impedance Spectroscopy and Transmission Line Modeling

To cite this article: Yongzhen Qi *et al* 2021 *J. Electrochem. Soc.* **168** 054502

View the [article online](#) for updates and enhancements.



 **240th ECS Meeting**
Oct 10-14, 2021, Orlando, Florida





**Register early and save
up to 20% on registration costs**

Early registration deadline Sep 13

REGISTER NOW



Interpreting Ionic Conductivity for Polymer Electrolyte Fuel Cell Catalyst Layers with Electrochemical Impedance Spectroscopy and Transmission Line Modeling

Yongzhen Qi,^{1,*}  Jiangjin Liu,^{2,3} Dinesh C. Sabarirajan,² Ying Huang,⁵  Andrea Perego,⁴ 
Andrew T. Haug,⁶ and Iryna V. Zenyuk^{1,2,4,5,**,z} 

¹Department of Mechanical and Aerospace Engineering, University of California Irvine, Irvine, California, United States of America

²Department of Mechanical Engineering, Tufts University, Medford, Massachusetts, United States of America

³Energy Conversion Group, Energy Technologies Area, Lawrence Berkeley National Laboratory, Berkeley, California 94720, United States of America

⁴Department of Chemical and Biomolecular Engineering; National Fuel Cell Research Center, University of California Irvine, Irvine, California, United States of America

⁵Department of Materials Science and Engineering, University of California Irvine, Irvine, California, United States of America

⁶3M Company, 3M Center, St. Paul, Minnesota, United States of America

A cathode catalyst layer containing optimally distributed ionomer is critical to reduce the platinum loading and increase its utilization in polymer electrolyte fuel cells. Here, electrochemical impedance spectroscopy (EIS) was used to measure effective ionic conductivity of pseudo catalyst layers (PCLs) at a relative humidity (RH) range of 50%–120%. These results are compared to previous work using the hydrogen pump (HP) method. EIS effective ionic conductivity results reported here are higher than those from the HP because in the HP set-up ionic pathways must be effectively connected through the PCL to be counted, whereas in the EIS measurement, ionomer segments that are in contact with the membrane but are not effectively connected all the way through the PCL can be detected. Double layer capacitances and effective ionic conductivities of Pt/C catalyst layers with various supports and ionomer to carbon (I/C) ratios were studied. High surface area carbon support resulted in a lower effective ionic conductivity compared to the graphitized carbon support due to worse ionomer dispersion. Effective ionic conductivities of Pt/C layers were compared to that of PCLs. On average, effective ionic conductivities of Pt/C layers were higher than PCLs because of possible carbon agglomeration within the PCLs.

© 2021 The Author(s). Published on behalf of The Electrochemical Society by IOP Publishing Limited. This is an open access article distributed under the terms of the Creative Commons Attribution Non-Commercial No Derivatives 4.0 License (CC BY-NC-ND, <http://creativecommons.org/licenses/by-nc-nd/4.0/>), which permits non-commercial reuse, distribution, and reproduction in any medium, provided the original work is not changed in any way and is properly cited. For permission for commercial reuse, please email: permissions@iopublishing.org. [DOI: [10.1149/1945-7111/abf96d](https://doi.org/10.1149/1945-7111/abf96d)]



Manuscript submitted November 17, 2020; revised manuscript received March 29, 2021. Published April 30, 2021. *This was paper 3743 presented during PRiME 2020, October 4–9, 2020.*

Supplementary material for this article is available [online](#)

Polymer electrolyte fuel cells (PEFCs) are promising clean energy conversion devices that use hydrogen as fuel.¹ A major application for PEFCs is in the automotive sector, where they are being developed as a more efficient, zero-emission replacement to internal combustion engines (ICEs) for automobiles, light duty and heavy duty vehicles, with additional applications as forklift power sources and electric vehicle range extenders.^{2,3} However, high cost of platinum (Pt) in the catalyst layers is a key challenge to bring PEFC vehicles fleet to a broad deployment. Current state-of-the-art fuel cell vehicles use >20 g of Pt per vehicle, however, to be comparable to current Pt use in ICE catalytic converters, less than 10 g of Pt per PEFC vehicle is needed.⁴ In PEFCs, cell performance is usually limited by the cathode electrode. Significant Pt amount is commonly used to overcome the slow kinetics of the oxygen reduction reaction (ORR),⁵ and transport resistances arising from oxygen and proton transport, and product water removal. To reduce Pt loading and improve its utilization on the cathode side, an optimal catalyst layer design is needed.⁶

A catalyst layer is comprised of Pt dispersed over a carbon support and ionomer such as perfluorosulfonated acid (PFSA).⁷ Ionomer content, distribution and optimization in cathode catalyst layer is critical to enable effective proton transport. Ionomer provides hydrophobicity to limit electrode flooding, without overly hindering local transport of oxygen to the Pt catalyst surface.^{8–10}

Several methods have been developed to understand ionomer distribution and ionomer conductivity during fuel cell operation. In 1980s Gottesfeld et al.¹¹ used electrochemical impedance spectroscopy (EIS) technique to measure ionic conductivity in catalyst layer using equivalent circuits to interpret the measurements. Later, Eikerling and Kornyshev first showed that the EIS response for the catalyst layer can be described by a one-dimensional transmission-line model (TLM).¹² Then Lefebvre and co-workers¹³ discussed the TLM for the operation under H₂/N₂ condition. Baker and collaborators included the catalyst layer thickness and relative humidity (RH) to investigate proton resistivity using a TLM.^{14–16} Jiang et al. expanded and tested a TLM capable of isolating and quantifying the resistance contributions from the membrane, the electronic components, and the membrane–electrode interfaces using EIS measurements.¹⁷ EIS measurements in combination with the TLMs have further increased in precision and capability.¹⁸ Obermaier et al. developed a one-dimensional TLM with additional elements describing the physics of species adsorption and side reactions making the model more comprehensive but at the same time requiring catalyst layer morphology as a model input.¹⁹

Previously, we used a hydrogen pump (HP) technique to measure effective ionic conductivity of the pseudo-catalyst layers (PCLs) without Pt over a relative humidity (RH) range of 50%–120%.²⁰ For the HP set up, multiple PCLs were placed between two membranes. A typical fuel cell anode and cathode catalyst layers were used on the outer side of each membrane. Then the DC potentials were applied to transport protons through the “membrane sandwich” from the anode to the cathode. We also developed an alternating current (AC) method using the same HP set-up and found that effective ionic conductivities of HP DC and HP AC obtained at low

*Electrochemical Society Student Member.

**Electrochemical Society Student Member.

^zE-mail: iryna.zenyuk@uci.edu

frequencies agree very well. At low frequencies AC method behaves as a DC method. The disadvantage of the DC or AC HP methods is that Pt cannot be used in the PCLs because hydrogen that crosses through the membrane will react and transport the current electrically. The advantage of the HP method is that it is very clear what the method is measuring: an effective ionic conductivity of ionomer segments that span the full thickness of the PCL.

In this work, we compare effective ionic conductivity of the PCLs from the AC HP method and H_2/N_2 EIS technique using standard fuel cell configuration. By comparing these two configurations and obtained ionic conductivities we want to better understand the strengths and weaknesses of each method and provide recommendation of which method better predicts a true effective ionic conductivity for the PCLs. Here, ionic conductivity for the PCLs with several ionomer to carbon (I/C) ratios was measured using H_2/N_2 EIS technique over a relative humidity (RH) range of 50%–120%. For the EIS study, we used a conventional fuel cell set-up with both PCLs and Pt/C as cathode layers and compared the results for two I/C ratios. Pt/C catalyst layers were used in this EIS study, since HP method could not be used to measure the real catalyst layer effective ionic conductivities. Furthermore, 2D model results using two effective ionic conductivities measured by EIS and HP are discussed and compared to determine which method is more practical. The study was extended to measurements of ionic conductivity of PCLs under different hot press conditions and ionomer content.

Experimental Methods

Materials and membrane electrode assembly (MEA) fabrication.—Ink processing and coating.—The catalyst inks and MEAs were made at 3 M company. Catalyst inks and carbon inks were prepared by mixing the components (typically 4–5 g of catalyst or carbon per batch) into an ink containing water and alcohols (such as nPa) at a ratio of 1:3. In each case (PCL or Pt/C) inks were prepared in a nitrogen (inert) enclosure. The carbon or catalyst powder was added first with water, followed by additional solvents and ionomer solution. After combining all the components, the catalyst ink or carbon ink was mixed by ball milling with 6 mm ceramic ZrO_2 beads for 48 hours. Using a 3 M company in-house pilot-scale manufacturing line, the catalyst layers or PCLs were coated atop a release film and dried in an inert atmosphere at temperatures up to 145 °C. Coatings of all catalyst types and I/C ratios were uniform and of high quality.

PCLs and the resulting MEAs.—For all the PCLs, 3 M 800 equivalent weight (EW) PFSA 20 μm membrane was used. Anode catalyst layer was laminated at 3 M and consisted of Tanaka TTK 10V50E (47 wt% Pt on Vulcan carbon), 3 M 800 EW ionomer at an I/C ratio of 0.8 and a Pt loading of 0.19 mg cm^{-2} . In-house at 3 M company roll-to-roll laminator was used to laminate 4 × 4 inch pieces of anode catalyst layer and membrane. The upper and the lower rolls of the laminator were heated to 177 °C and 100 psi was applied to the roll drums. Protective PET film was applied outside of the top and bottom of the assembly. The package was then sent through the laminator at 0.37 m min^{-1} . After the lamination step, PET protective film and release liners were removed leaving a half-catalyst-coated membrane (CCM) for testing. The cathode layers were single layers of the PCLs made by 3 M company with Vulcan XC72 carbon black and 3 M 800 EW PFSA ionomer with I/C ratios of 0.3, 0.6, 1.0, 1.2 and 1.4. These PCLs I/C ratios were chosen to enable comparison with our previous work²⁰ but also to represent the range typically used in commercial applications. The measured thicknesses of the cathode PCLs were 8 μm , 11 μm , 12 μm and 14 μm for PCLs with I/C ratio of 0.3, 0.6, 1.0, 1.2 and 1.4, respectively. The cathode PCL was hot pressed onto the other half of the CCM and sandwiched between Kapton® polyimide sheets of 25 μm thickness, masking an active area of 5 cm^2 . The hot press

condition was 140 °C and 2000 kg total pressure. The duration of hot-press procedure was 3 min.

MEAs with Pt/C.—The MEAs with Pt/C layers as cathode catalyst layers were manufactured at 3 M company with similar procedure described above. Both anode and cathode catalyst layer were placed on both sides of membrane and were laminated at 3 M using the same conditions as above. In this study Pt/C loading was kept at 0.2–0.3 mg_{Pt} cm^{-2} , whereas ionomer fraction and type of carbon support were varied. For all the MEAs the ionomer was 3 M 800 EW PFSA. The anodes for all the MEAs consisted of 0.10 mg Pt/ cm^2 loading, 50 wt% Pt on graphitized carbon ($\sim 80 m^2 g^{-1}$ surface area), 3 M 800 EW I/C = 0.8 ionomer. 3 M 800 EW 20 μm membrane was used in all of the MEAs. The cathode catalyst layers thicknesses were measured to be at 8 μm . Table 1 shows the specifications for the four MEAs.

Sigracet SGL 29 BC was used as the gas diffusion layer (GDL). Teflon fiberglass sheet layer of 180 μm thickness was used on both sides between MEA and bipolar plate as hard-stop gasket to achieve a 20% compression of the GDL. Scribner hardware with 5 cm^2 flow-field with a single serpentine of 1 mm × 1 mm land and channel was used.

Experimental testing procedure.—The experiments were done using the Biologic SP150 potentiostat and the Scribner 850e fuel cell hardware. Figure 1a shows a schematic of the EIS experimental set up used in this study. First, MEA surface cleaning step was done for 1 hour by holding the cell temperature at 60 °C with the RH of 100%, with 0.25 slpm H_2 and 0.25 slpm N_2 on the anode and cathode, respectively with no applied backpressure. Then using the same gases and gas flow-rates, 100 mV s^{-1} sweep rate was applied between 0.05 and 1.1 V for 100 cycles. After which, the cell temperature was increased to 80 °C and the inlet gases temperature was set to 64 °C dewpoint (50% RH) on both anode and cathode sides. Anode and cathode back pressures were set to 100 kPa (200 kPa absolute). The gases were then set to 0.25 slpm H_2 and 0.75 slpm N_2 at the anode and cathode, respectively.

The RH allowed to equilibrate for 30 min by only purging gases at open circuit voltage (OCV). For the chosen potential range ($>0.2 V$), the H_2 crossover currents will not influence the AC impedance signal significantly.¹⁴ In other works, potentials were set to 0.45–0.5 V to collect EIS data.^{19,21} Here, after RH equilibration, the impedance was measured from 0.2 to 0.6 V in increments of 0.1 V. After 5 min hold at the selected voltage, an AC perturbation was applied to perform EIS. The AC perturbation potential with an amplitude of 10 mV was applied over a frequency range from 500 kHz to 100 mHz. Recording rate was set at 8 points per decade. AC impedance measurements at each RH were repeated three times to ensure reproducibility. In this work, effective ionic conductivities were measured for a potential range from 0.2 to 0.6 V. We found that effective ionic conductivity was independent from the applied potentials in the Supplementary Material (SM), Fig. S1 (available online at stacks.iop.org/JES/168/054502/mmedia). All the effective ionic conductivities shown in this work are from measurements at an applied potential of 0.2 V.

Scanning electron microscope (SEM) sample preparation and imaging.—The cross-sectioned samples were broken using liquid nitrogen and mounted on 90° SEM specimen mounts. Samples were imaged with a FEI Magellan 400 scanning electron microscope detector operating at 10 kV accelerating voltage. Images were taken in secondary electron imaging mode. The elemental mapping was gained by energy-dispersive X-ray spectroscopy (EDS) with Oxford Silicon Drift Detector and controlled by AZtec Software.

Data analysis and model fitting methods.—Equivalent circuit model.—Figure 1 shows a schematic of the PEFC set-up and two equivalent circuits. Figure 1b represents the TLM of one single pore

Table I. Cathode side for four MEAs used in this study.

	Cathode I/C ratio	Cathode Pt loading (mg cm^{-2})	Cathode carbon support	Cathode catalyst layer thickness (μm)
MEA 1	0.4	0.29	Graphitized carbon (GrC)	8
MEA 2	0.9	0.21	Graphitized carbon (GrC)	8
MEA 3	1	0.24	High-surface area carbon (HSC)	8
MEA 4	1.2	0.205	Vulcan XC72, medium surface area carbon (MSC)	8

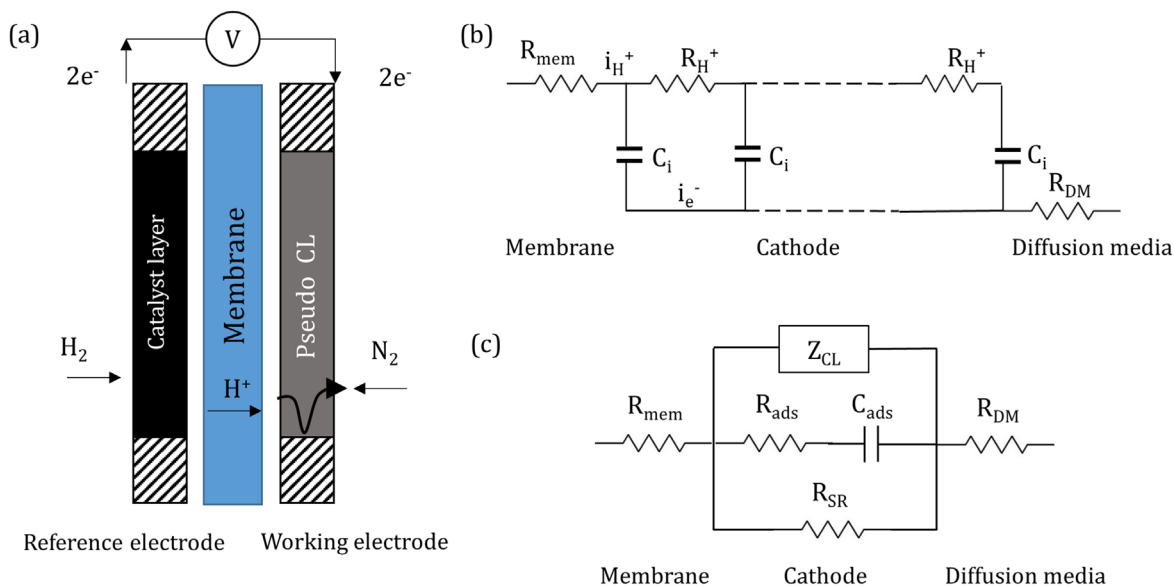


Figure 1. (a) Schematic of the set-up for H_2/N_2 EIS, (b) conventional TLM for a single pore and (c) the total equivalent circuit used in this study, which is adopted from Ref. 19.

filled with ionomer, and it is considered as consisting of many parallel capacitors C_i connected with proton transport resistors R_{H^+} between each capacitor. According to deLevie's model, the impedance of each pore (Fig. 1b) in the catalyst layer can be considered as:

$$Z_{deLevie} = (R_0 Z_0)^{1/2} \coth \left(l \sqrt{\frac{R_0}{Z_0}} \right) \quad [1]$$

where, R_0 is the electrolyte resistance for a unit length, Z_0 is the interfacial impedance for unit length, and l is the length of each pore.¹⁸

In contrast to Obermaier et al.,¹⁹ which considered the pore size distributions, and a specific TLM for each pore, we simplify the entire catalyst layer to be represented by the TLM of a single cylindrical pore with representative parameters. Hence the impedance of the catalyst layer can be represented as:

$$Z_{CL} = (R_0 Z_0)^{1/2} \coth \left(l \sqrt{\frac{R_0}{Z_0}} \right) \quad [2]$$

$$R_0 = \frac{1}{\sigma_{eff} \times A} \quad [3]$$

$$Z_0 = \frac{1}{A_S \times A \times \omega \times C_{DL} \times j} \quad [4]$$

where A is the active area of the cell, A_S is the specific surface area, i.e. $1.5 \times 10^7 \text{ m}^{-1}$,²² σ_{eff} is the effective ionic conductivity of the catalyst layer, ω is the angular frequency, C_{DL} is the double layer capacitance and j is the unit of imaginary number.

Figure 1c shows the equivalent circuit adopted from Obermaier et al.¹⁹ The model neglects the impedance response of the anode catalyst layer, as it is shorted by the fast hydrogen oxidation reaction. Also because of the absence of the reactive gas there are no Faradaic resistances in the cathode catalyst layer. Z_{cl} represents the impedance of the cathode catalyst layer which can be determined using the TLM. The capacitors in the TLM represent the contacts between ionic phase and electronic phase, i.e. the contact between electrolyte and Pt surfaces or carbon surfaces. In view of these, ion species adsorption and side reactions which can affect the measurements should be considered.

Hence, the resistor and capacitor of ion species adsorption, specifically sulfonic acid group adsorption, and resistor of side reaction, specifically hydrogen crossover are added into the cathode equivalent circuit. In Fig. 1c, the adsorption capacitor, C_{ads} and adsorption resistor, R_{ads} are connected in series. They represent the sulfonic acid groups adsorption of ionomer on Pt electrocatalyst and other species adsorptions. Side reactions term, R_{SR} , represents impedance caused by hydrogen crossover through membrane and possible presence of trace amounts of oxygen.

Overall, the modeled equivalent circuit of the cell in this paper is shown in Fig. 1c. It consists of three components in series: membrane resistance, the impedance of cathode catalyst layer and the electrical resistance of the diffusion media R_{DM} . The equivalent circuit of cathode catalyst layer is a sum of parallel connections of impedance of proton transport Z_{CL} , adsorption resistance R_{ads} and capacity C_{ads} in series, and the side reaction, R_{SR} . R_{mem} denotes the sum resistance of membrane ion transport resistance and contact resistances.

Based on the total equivalent circuit shown (Fig. 1c), total impedance and impedance of the cathode catalyst layer is considered as:

$$R_{tot} = R_{mem} + R_{cath} + R_{DM} \quad [5]$$

$$\frac{1}{R_{cath}} = \frac{1}{Z_{cl}} + \frac{1}{R_{ads} + Z_{ads,C}} + \frac{1}{R_{SR}} \quad [6]$$

The TLM fitting code was written using MATLAB. For the fitting, the input parameters include cell area A , specific area A_S , angular frequency ω , real resistance from Nyquist plot Z_{real} , imaginary resistance from Nyquist plot Z_{img} , and the length of catalyst layer, l . Effective ionic conductivity was and output of the model and was obtained by fitting the impedance spectroscopy data.

Double layer capacity calculation.—Double layer capacity was calculated from the collected EIS data. Iden and Ohma²¹ utilized the relationship among double layer capacity, frequency and imaginary impedance:

$$-\frac{1}{\omega \times Z_{img}} = \frac{1}{\omega^2 \times R_{ct}^2 \times C_{dl}} + C_{dl} \quad [7]$$

where ω is the angular frequency, Z_{img} is imaginary part of impedance, R_{ct} is the resistance of the charge transfer, which is a consequence of hydrogen crossover through the membrane and C_{dl}

is the double layer capacitance. In this paper, $-\omega^{-1} \times Z_{\text{img}}^{-1}$ was plotted as a function of ω^{-2} , and C_{dl} was then obtained by extrapolating to $\omega^{-2} = 0$.

Results

SEM observations.—Figure 2 shows SEM cross-section of the PCL, where good adhesion between PEM and a PCL was observed after hot press. We observed a PCL to be of uniform thickness. EDS results show distribution of platinum (Pt) and carbon (C) within the catalyst layer and PCL, respectively. Pt particles are seen in anode catalyst layer region above membrane, and we confirm that in the cathode PCL there is carbon but no Pt.

It is critical to know the influence of the interface between PCLs and membrane on effective ionic conductivities. In Fig. S2, we compare the effective ionic conductivity of PCLs that were physically pressed and hot pressed onto the membranes for both low and high I/C ratios. From the results, the effective ionic conductivities of hot-pressed PCLs are much higher than the PCLs without hot-pressing. However, the PCL effective ionic conductivities are independent to the hot press conditions.

PCLs conductivity.—Figure 3 shows the Nyquist plots for the PCLs with I/C ratios of 0.3, 0.6, 1.0 and 1.4 at RHs of 50, 75, 100 and 125%. An example of the fitting of the PCL Nyquist plot is shown in the SM, Fig. S3. Overall, a good fit was obtained for Nyquist plots using the TLM. The HFR shown in Nyquist plots is the summation of the contact resistances and membrane ion transport resistance. The HFR decreased with increasing RH for all four I/C ratios, which is due to the increased conductivity of a more hydrated membrane and decreased contact resistance between membrane and catalyst layer. We see a decreased length of the 45° segment at intermediate frequencies with increased RH and I/C ratio. Qualitatively, a 45° segment on Nyquist plot represents one-third of proton transport resistance, $R_{\text{Cl}}/3$.¹³ Decrease in the length of a 45° segment is due to proton transport resistance decreasing and proton conductivity increasing with increased ionomer and water content. HFR is smaller when the PCL I/C ratio is higher due to better contact between the PCL and membrane. An outlier is observed for the HFR of the PCL with I/C ratio of 1.4, which has higher HFR and does not follow the trend of reduced HFR with increase in I/C. We believe that at this high I/C ratio, significant amount of ionomer is present at the surface of the PCL, thus reducing the electric contact resistance between the PCL and micro-porous layer.

PCLs effective ionic conductivities and comparison of EIS and hydrogen pump set-up.—The effective ionic conductivity of PCLs with different I/C ratios is plotted in Fig. 4a. A clear trend is observed, where effective ionic conductivity increases with increase in ionomer content and RH. Effective ionic conductivity increased 3.5–21 times when RH increased from 50% to 120%. The largest increase in conductivity was observed for I/C of 0.3, where effective ionic conductivity was $7 \times 10^{-5} \text{ S cm}^{-1}$ for RH of 50% and increased to $1.5 \times 10^{-3} \text{ S cm}^{-1}$ for RH of 120%. For I/C of 1.4, a smaller increase in effective ionic conductivity was observed, from $8.96 \times 10^{-3} \text{ S cm}^{-1}$ at 50% RH to $3.29 \times 10^{-2} \text{ S cm}^{-1}$ at 120% RH. For a constant RH the largest increase in effective ionic conductivity was observed at 50% RH, where effective ionic conductivity increased from 7×10^{-5} to $8.96 \times 10^{-3} \text{ S cm}^{-1}$ when I/C increased from 0.3 to 1.4.

Figure 4b displays the effective conductivities measured by EIS data fitting with TLM and that measured with AC hydrogen pump (HP) set-up reported by our earlier study, here referred as AC HP.²⁰ In that study, as shown by Fig. 5a, the PCLs were sandwiched between two membranes and hydrogen pump experiment was conducted where hydrogen is reacted on the anode to form protons which are transported across the membrane-PCLs-membrane

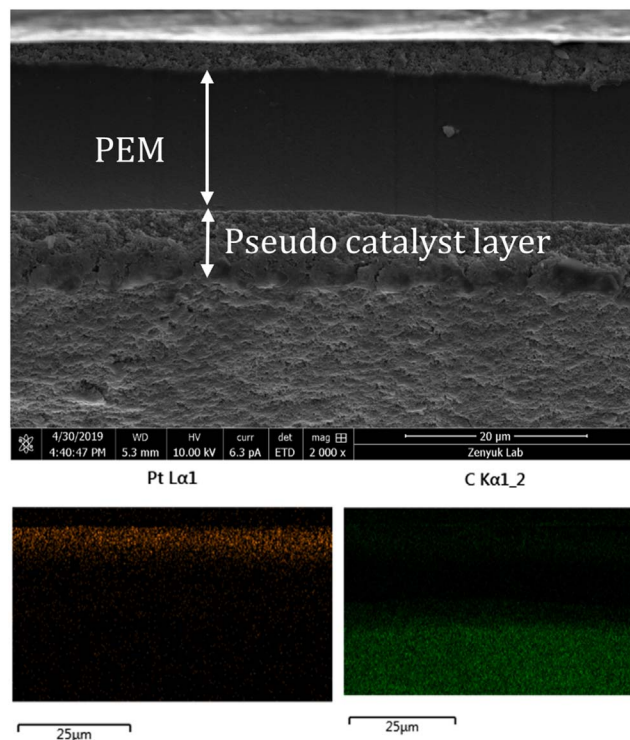


Figure 2. Cross section SEM image of a PCL pressed onto the membrane with I/C ratio of 0.6 where PCL is hot pressed onto a PEM (top), Pt and C EDS mapping (bottom).

assembly, and finally recombined into H_2 on the cathode side. Both DC and AC methods were used to fit the data in the HP set-up and they showed good agreement. Here we replot only the AC data from our earlier work, Sabarirajan et al.²⁰ and omit DC HP data, for the purpose of being concise. A large discrepancy between EIS and AC HP results is observed at low RH, and the effective ionic conductivity measured by EIS is 10–65 times higher than that measured by AC HP. At high RH condition, EIS measured conductivity is about 0.5–3 times that of AC HP measurements. For example, for PCL with I/C of 0.6, with RH increased from 50% to 120%, EIS measured effective ionic conductivity increased from $4.26 \times 10^{-4} \text{ S cm}^{-1}$ to $2.46 \times 10^{-3} \text{ S cm}^{-1}$. In contrast, AC HP measured effective ionic conductivity increased from $3.83 \times 10^{-5} \text{ S cm}^{-1}$ to $4.82 \times 10^{-3} \text{ S cm}^{-1}$. For the highest I/C of 1.4, EIS measured effective ionic conductivity increased from $8.96 \times 10^{-3} \text{ S cm}^{-1}$ to $3.29 \times 10^{-2} \text{ S cm}^{-1}$ with RH increased from 50% to 120%. And AC HP effective conductivity increased from $1.45 \times 10^{-4} \text{ S cm}^{-1}$ to $1.06 \times 10^{-2} \text{ S cm}^{-1}$. Figure 4c shows the ratio between the EIS and AC HP effective conductivity values. Figure S4 shows this ratio on the logarithmic scale. At high RH the ratio approaches the value of 0.5–3. This is indicative that the two methods converge at high RH. However, as RH is decreased the ratio between the two conductivity measurements increases, for example, at 75% RH for I/C 0.6, 1.0 and 1.4 the conductivity ratios are 4, 8.56 and 20.6, respectively. Whereas for RH of 50% the effective ionic conductivity ratios were 11.1, 18.2 and 61.9, respectively.

The definition of effective ionic conductivity is as following:

$$\sigma_{\text{eff}} = \frac{\epsilon}{\tau} \sigma \quad [8]$$

where, σ is the bulk conductivity, ϵ is the volume fraction of ionomer in the PCL which can be determined according to Liu et al.'s work¹⁵ and τ is the tortuosity factor. The same type of ionomer was studied, i.e. bulk conductivity σ is the same for EIS and HP,

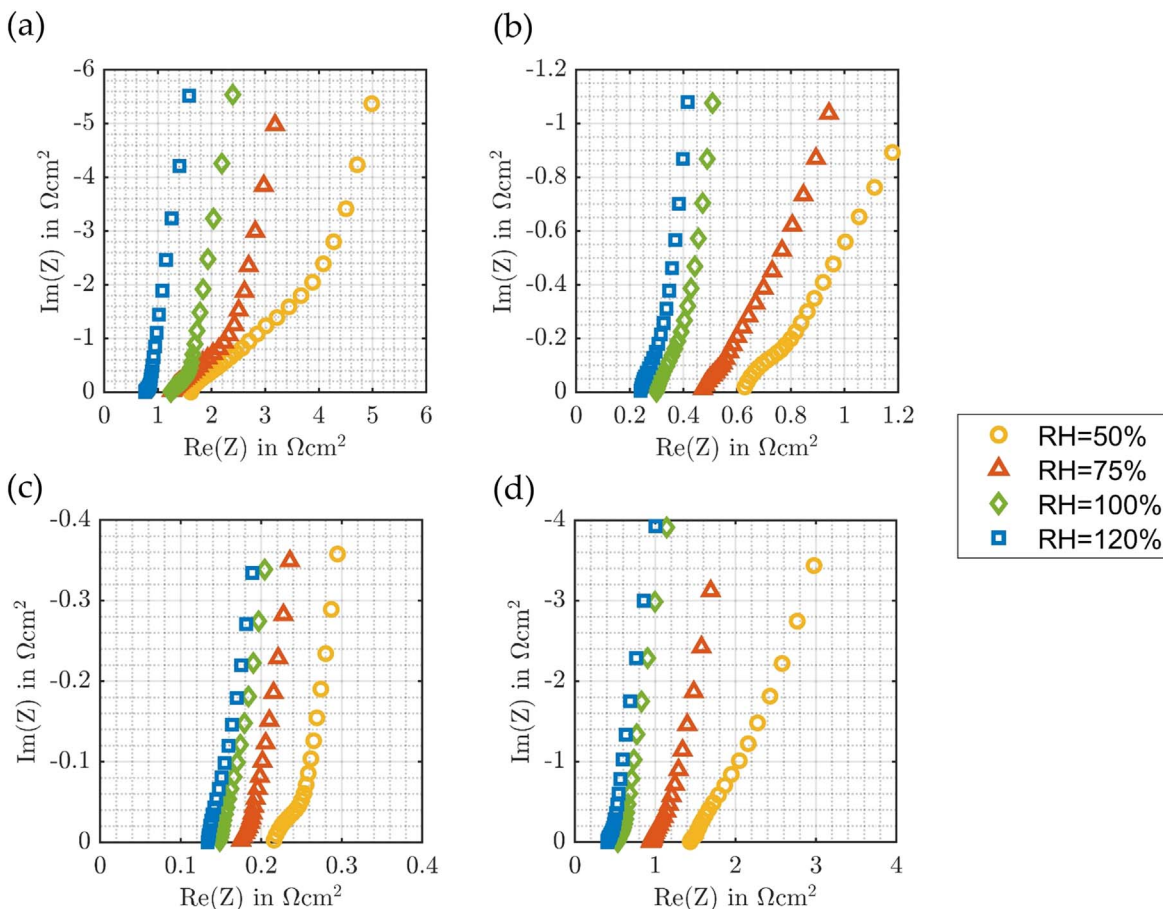


Figure 3. Nyquist plots over the RH range of 50–120% at an applied potential of 0.2 V for PCLs with an I/C ratio of: (a) I/C = 0.3, (b) I/C = 0.6, (c) I/C = 1.0, and (d) I/C = 1.4.

therefore, we can represent the ratio between the two effective ionic conductivities as:

$$\frac{\sigma_{EIS}}{\sigma_{HP}} = \frac{\epsilon_{EIS} \tau_{HP}}{\epsilon_{HP} \tau_{EIS}} \quad [9]$$

where, $\frac{\epsilon_{EIS}}{\epsilon_{HP}}$ is equal to 1, as in both HP set-up and in this conventional set-up the equilibration time was sufficiently high for ionomer RH to be at equilibrium with the inlet gas RH. As we will explain in the next paragraphs, the HP technique captures only transport in ionomer that is effectively connected through the full thickness of the PCL. The ratio of tortuosity factors, $\frac{\tau_{HP}}{\tau_{EIS}}$ again is related to the degree of ionomer connectivity.

For the modeling studies, tortuosity, τ_1 , is more useful quantity than tortuosity factor, as it can be directly input into the computational model. The two quantities are related as:

$$\tau_1 = \tau^{0.5} \quad [10]$$

We reported in our earlier study the values of the tortuosities for the AC HP method.²⁰ Here, these values are reproduced by Figs. 4d–4e along with the calculated values from the EIS method under 50% RH and 100% RH for I/C = 0.6, I/C = 1.0 and I/C = 1.4. At 50% RH, tortuosity from AC HP were in the range from 3.5 to 6.5, whereas those calculated with the EIS method were 0.6 to 2. The high tortuosities predicted by AC HP method might be due to carbon agglomeration in the PCL, as will be discussed later. This agglomeration might be prevented with the right selection of solvents and mixing procedure for the ink, as well, as addition of Pt, as done for catalyst layers. At 100% RH, shown by Fig. 4e AC HP tortuosities

were between 1–2, whereas those measured with the EIS were in the range from 0.5 –1. For both RH, EIS method shows tortuosity decreasing with increase in I/C ratio. The values of tortuosity for AC HP and EIS are closer at 100% RH compared to 50% RH.

Figure 5 shows the schematic of experimental set-ups for AC HP and EIS measurements. In the AC HP measurement (Fig. 5a), hydrogen was used on both the anode and cathode sides, and a DC voltage from OCV to –0.4 V was applied across the cell. In the HP DC set-up, for protons to be measured as current they must completely cross the PCL from the anode to cathode. Therefore, as shown by Fig. 5a, if the ionomer pathways are not effectively connected through the PCL then protons will not readily conduct through these sections, then those ionomer segments will not be detected. These dead-end pathways will increase the tortuosity factor in the DC method. The loss of connectivity is especially pronounced at low RH and low I/C ratios, where ionomer regions are no longer connected by liquid water. Gostick and Weber²³ have shown that in a typical resistor network model of ionomer mixed with non ionically conductive support, ions flow through only very few preferential ionomer pathways. In the EIS measurement set-up (Fig. 5b), protons will be transported through all of the ionomer in contact with the membrane. In the EIS measurement the ionomer does not need to be effectively connected through the whole thickness of the catalyst layer. As the schematic shows, the difference between the HP and EIS methods is most pronounced at low RH, and it has been confirmed by effective ionic conductivity measurements.

Effective ionic conductivity and volume-averaged fuel cell models.—Thus, the question arises: which tortuosity and effective ionic conductivity should be used within the fuel cell models to

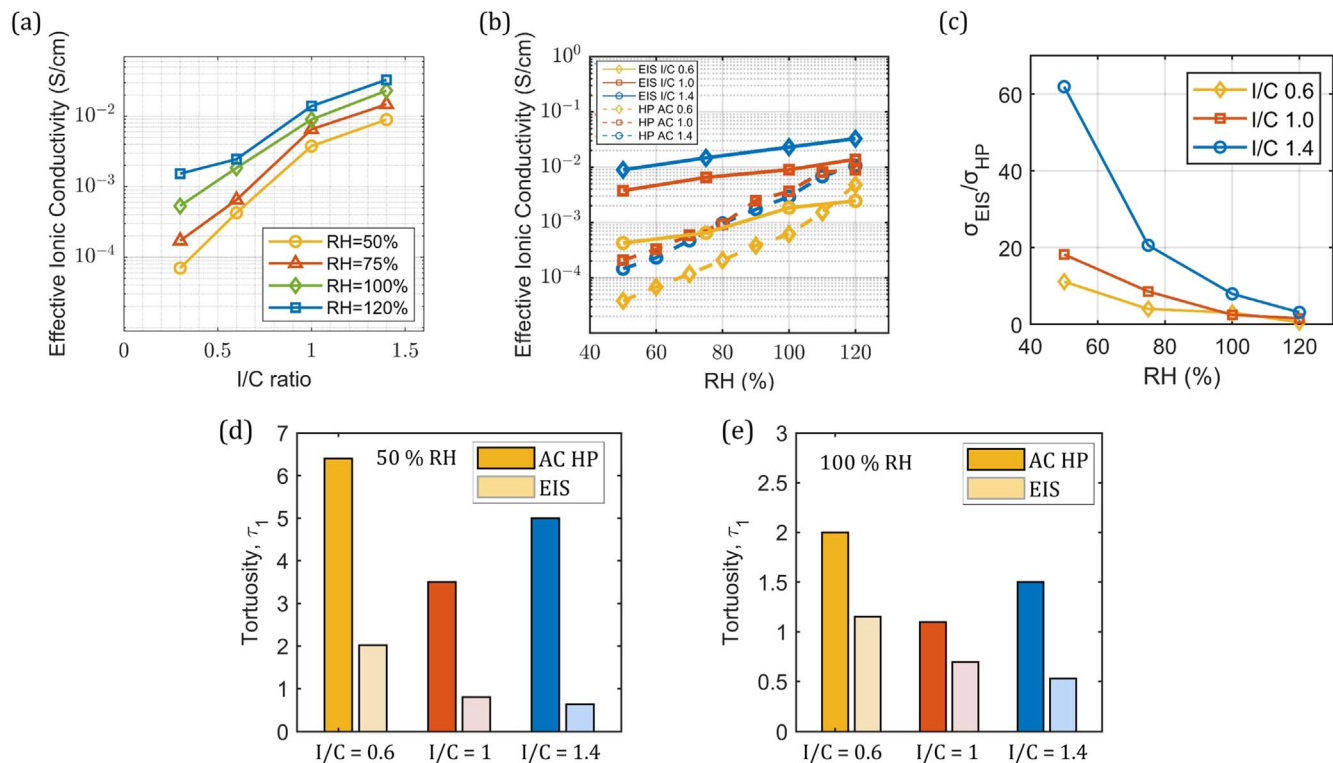


Figure 4. (a) Effective ionic conductivity for PCLs for a range of I/C ratios and RH from 50 to 120%, (b) comparison of PCLs effective ionic conductivity measured by EIS (solid line) and AC HP (dash line), where the AC HP data is reproduced from our earlier study,²⁰ (c) the ratio between the PCLs effective ionic conductivities measured by EIS and HP as a function of RH. Tortuosity values calculated by using effective ionic conductivities of PCLs measured by EIS and AC HP under (d) 50% RH and (e) 100% RH for I/C = 0.6, I/C = 1.0 and I/C = 1.4.

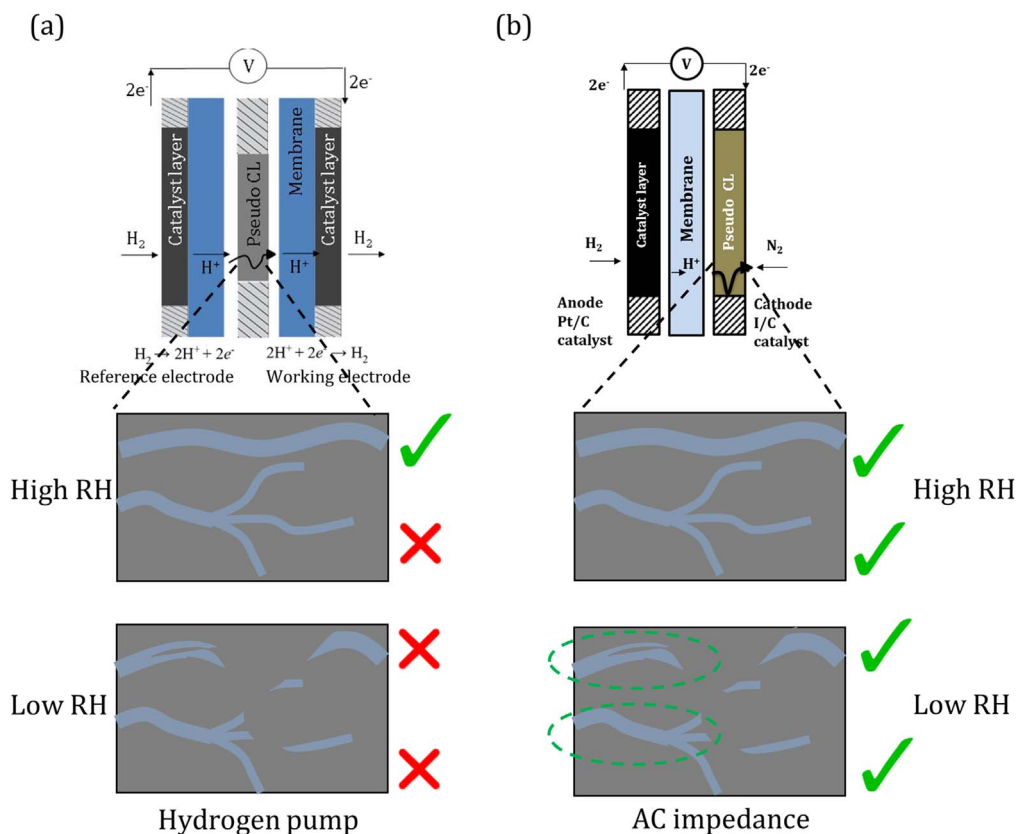


Figure 5. Schematics of (a) AC or DC HP and (b) EIS experimental set ups and a representative schematic of ionomer percolation through the PCLs at low and high RH.

accurately represent catalyst layer properties? Recent computational work by Cooper and co-authors²⁴ similarly compared equivalent to our HP DC method (called restricted diffusion method eRDM) and AC method (called symmetric cell method (eSCM)) using battery electrodes. They similarly pointed out the difference between the two methods is mostly in counting or not counting dead-ended pores in their case and ionomer segments in our study. They concluded that the AC method (eSCM in their study) is more accurate, as for battery to function one does not need pores (filled with electrolyte) connectivity through the layer. Fuel cell catalyst layers need both protons and oxygen reactants that come from different sides of the catalyst layer for the ORR to occur, thus the conclusion of which tortuosity to use or which method is more precise is not as straight forward.

Here, we used a 2D cross-section multiphysics model of PEFC reported previously²⁵ to simulate PEFC polarization behavior for 10 μm thick catalyst layer with I/C of 1 and RH of 50% and 75%. As shown in Fig. 6, at both RHs, the current density is higher when σ_{EIS} was used in the model. For example, at 50% RH, it increases from 0.74 A cm^{-2} to 1.08 A cm^{-2} at 0.4 V when σ_{HP} and σ_{EIS} were used in the model, respectively. The only difference in the models is the effective ionic conductivity of the cathode catalyst layer. Therefore, the increase in the current densities is due to the lower ohmic loss in the cathode catalyst layer when σ_{EIS} was used. Similarly, the current density increases from 50% RH to 75% RH for both methods due to the increased effective ionic conductivity. At 50% RH, σ_{HP} is very low and the current density is primarily limited by ion transport in the cathode catalyst layer. As a result, when RH increases from 50% to 75%, the current density increased significantly. As a comparison, when σ_{EIS} was used in the model, current density only increases a small amount when RH increases from 50% to 75%. The reason is that in this case the ion transport is no longer the limiting factor, though the ohmic loss is still reduced when effective ionic conductivity increases.

Volume-averaged models utilize effective ionic conductivity values. These can be either directly fit for different temperatures and RHs, or they can be expressed as inherent ionomer conductivity adjusted with ionomer volume fraction and tortuosity, which will become effective ionic conductivity. Thus, if the EIS measurement is used, and the appropriate fits are created for the model to use then the model will most likely overapproximate the fuel cell performance because volume-averaged modeling approach does not account for the portion of the catalyst layer, where ionomer did not effectively connect through, and hence where Pt will not be connected via ionomer or water domains (especially at low RH operating conditions). The DC method will almost certainly underapproximate fuel cell performance, however, it is a good metric for the through-thickness catalyst layer effective ionomer connectivity. More work is required to properly integrate these effective ionic conductivity measurements into the fuel cell model, here we provided just a very basic illustrations of impact of effective ionic conductivity on polarization behavior of the PEFC. An alternative approach would be to computationally measure the EIS spectra in the model and fit the experiment data.

Comparison of effective ionic conductivity and double layer capacitances for the Pt/C catalyst layers.—Effective ionic conductivities for the Pt/C catalyst layers (Table I) were measured. For each MEA, three cells were built and tested, to ensure reproducibility. GrC carbon support (MEA 1 and MEA 2) has almost no internal porosity, which results in a low total surface area, where all the Pt particles distribute on the surface of the support. For MEA 3, according to Nagappan et al.,²⁶ high surface area carbon (HSC) support has around 3–5 times higher total surface area than Vulcan carbon support due to its high internal porosity. Figure 7a shows the effective ionic conductivities for MEA 1 and MEA 2 (properties defined in Table I). The Nyquist plots at 0.2 V and the corresponding equivalent circuit fits are shown in the SM, Figs. S6 and S7. The

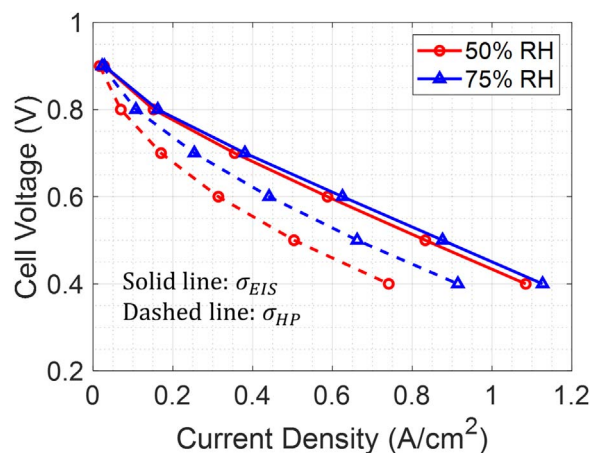


Figure 6. Polarization curves from PEFC model for I/C = 1 at 50% and 75% RH by using the effective ionic conductivity from EIS and HP AC measurements. A significant difference in current density is observed, which is due to the much higher effective ionic conductivity.

error bars in Fig. 7a show the variations of three cell builds. MEA 1 and MEA 2 have the same GrC support but different I/C ratios and slightly different Pt loadings. Effective ionic conductivity measurements for applied potentials from 0.2 to 0.6 V are shown in the SM, Fig. S5. The following trend in the effective ionic conductivity is observed: MEA 1 (I/C = 0.4) < MEA 2 (I/C = 0.9). One reason is that the ionomer connectivity is lower at low I/C ratios. Another reason is that at lower I/C ratios, carbon agglomeration is promoted, as observed in literature with small angle X-ray scattering.²⁷ Carbon agglomeration will also increase ionomer tortuosity and reduce proton conductivity.

Figure 7c shows the double layer capacities calculated by Eq. 7 for MEA 1 and MEA 2 at 100% RH. Double layer capacity at a specific RH depends on both I/C ratio and carbon support. MEA 1 with I/C ratio of 0.4 showed the lowest double layer capacity of 46 mF cm^{-2} due to lower ionomer content and lack of the carbon support's internal pores. MEA 2 with I/C 0.9 showed slightly higher double layer capacity of 51 mF cm^{-2} compared to MEA 1. At 100% RH we do not expect these double layer capacitances to be drastically different between MEA 1 and MEA 2 because condensed liquid water will be present and carbon black-water interface, as well as Pt-water interface will be counted towards the double layer capacity.

Figure 7b shows effective ionic conductivities for MEA 2 and MEA 3 (properties reported in Table I). The Nyquist plots at 0.2 V and corresponding equivalent circuit fits are shown in the SM, Figs. S6 and S7. MEA 2 and MEA 3 have similar I/C ratios at around 1 and Pt loadings of 0.21–0.24 mg cm^{-2} , but different carbon supports. At low RH, MEA 3 with the HSC support showed lower effective ionic conductivity. It was shown recently by Ramaswamy et al.²⁶ that surface area of smaller meso-pores (> 8 nm) of the carbon support determines the continuity and uniformity of the ionomer distribution in the catalyst layer. The GrC carbon support in MEA 2 has less to no meso-pores compared to the HSC used in MEA 3, which results in a larger effective ionic conductivity of MEA 2. At high RHs of 120%, for MEA 3 with HSC support, internal pores will be filled with condensed water resulting in a better continuity of ionic pathways and creating more ionic pathways especially for those Pt particles inside the internal pores of the HSC support. Therefore, similar effective ionic conductivity was observed between MEA 2 and MEA 3. Figure 7d shows the double layer capacities for MEA 2 and MEA 3 with 100% RH condition. MEA 3 showed higher double layer capacity of 119 mF cm^{-2} at 100% RH. This is due to higher surface area of carbon and better dispersion of Pt nanoparticles on carbon support. MEA 2 with GrC support showed more than 2 times lower double layer capacity compared to

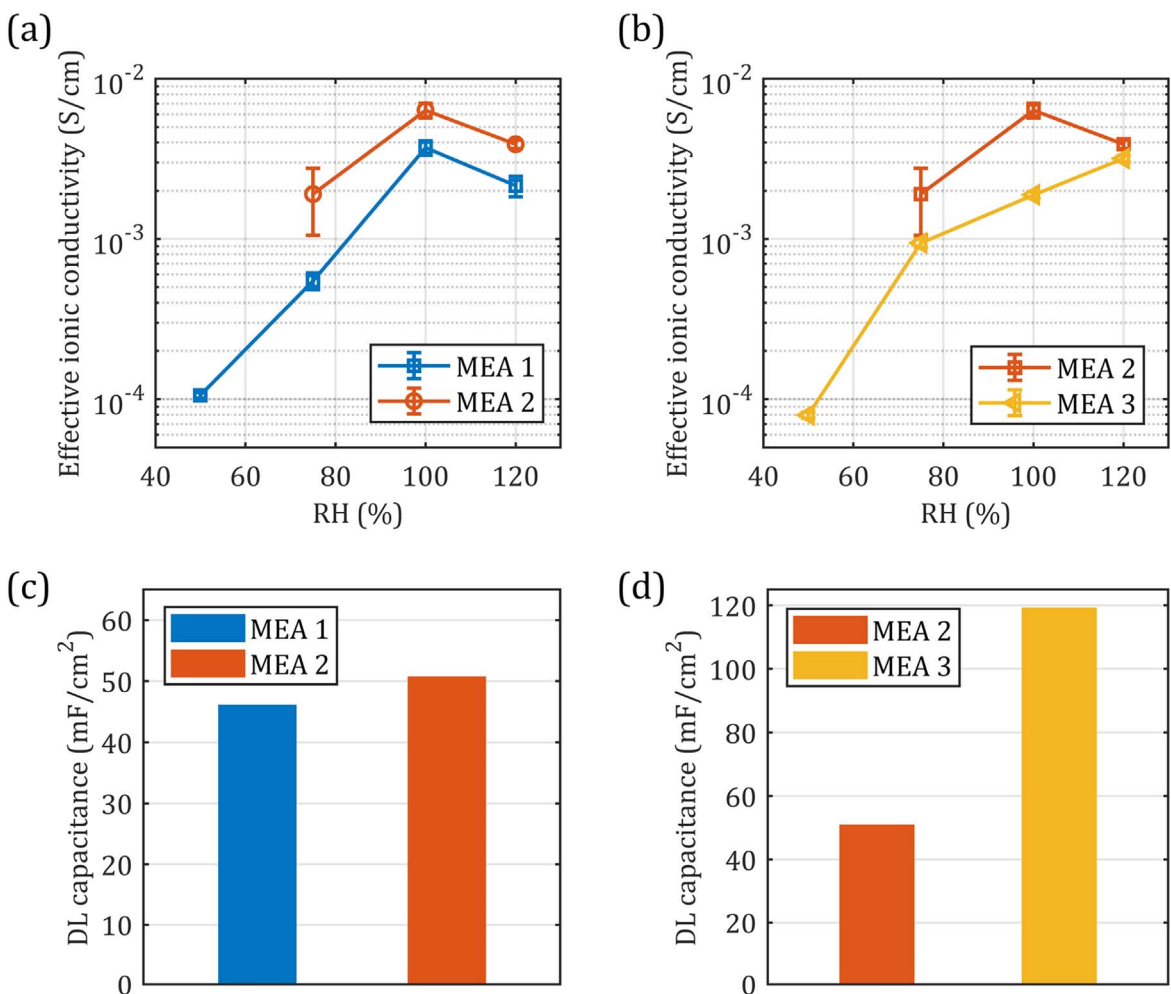


Figure 7. (a) Effective ionic conductivities for catalyst layers of MEA 1 and MEA 2 in the RH range from 50% to 120% (b) effective ionic conductivities for catalyst layers of MEA 2 and MEA 3 in the RH range from 50% to 120% (c) double layer capacitances for catalyst layers of MEA 1 and MEA 2 at 100% RH. (d) double layer capacitances for catalyst layer of MEA 2 and MEA 3 at 100% RH.

MEA 3 due to GrC support having lower surface area compared to HSC support and due to potentially Pt be more agglomerated on GrC support.

Comparison of effective ionic conductivity between PCL and Pt/C catalyst layer.—Figure 8 shows the effective ionic conductivities comparison between PCLs (without Pt) with I/C ratio of 0.3 and 1.2 and Pt/C layer (MEA 1 and MEA 4 in Table I) with I/C ratio of 0.4 and 1.2 with the same carbon supports under different RH conditions from 50% RH to 120% RH. For each I/C ratio, three cells were built and tested. Three repeated experiments were conducted and the variations were evaluated and shown by the error bars. For low I/C ratio of 0.3–0.4 (Fig. 8a), effective ionic conductivity for the PCL increased from 1.18×10^{-4} S cm⁻¹ at 50% RH to 1.79×10^{-3} S cm⁻¹ at 120% RH, whereas Pt/C layer effective ionic conductivity increased from 1.03×10^{-4} S cm⁻¹ at 50% RH to 2.26×10^{-3} S cm⁻¹ at 120% RH. Above 50% RH, Pt/C layer has higher effective ionic conductivity because at these low I/C ratios the carbon support tends to agglomerate when Pt is not present, increasing ionomer tortuosity and reducing effective conductivity.

Figure 8b shows the effective ionic conductivities comparison for high I/C ratio of 1.2. Effective ionic conductivity of the PCL increased from 5.76×10^{-4} S cm⁻¹ at 50% RH to 1.94×10^{-3} S cm⁻¹ at 120% RH, whereas Pt/C layer effective ionic conductivity increased from 2.11×10^{-4} S cm⁻¹ at 50% RH to 4.97×10^{-3} S cm⁻¹ at 120% RH. At 120% RH Pt/C layer has 2.2 times higher

effective ionic conductivity than PCL, whereas at 50% RH it is 2 times lower. The conductivity differences between the PCL and Pt/C is not as obvious as for the low I/C ratio. Carbon agglomeration may still occur in the PCL but its impact on ionomer distribution for higher ionomer content layer is not as clear. The presence of Pt nanoparticles reorients ionomer also changes the size of agglomerates, resulting in the effective ionic conductivity change. And in the full range of RH, effective ionic conductivities of Pt/C layers experience a greater increase compare to PCLs due to hydrophilicity of Pt particles, in other words, more water content is attracted to Pt particles and help proton transport.

Conclusions

PCLs effective ionic conductivities were measured in a conventional PEFC set-up, using EIS collected in H₂/N₂ environment and a RH range from 50 to 120%. The EIS was fitted with the TLM for the PCLs with I/C 0.3, 0.6, 1.0, 1.2 and 1.4. PCLs effective ionic conductivity increased with I/C ratio and RH because ionomer and water provided more ionic pathways for proton transport. Ion conductivities measured using EIS and previously reported with AC HP method were compared for the PCLs with I/C of 0.6, 1.0 and 1.4. In AC HP set-up, only ionomer that is effectively connected through the full catalyst layer thickness carries proton current. The remaining of the ionomer pathways that are dead-ended increase tortuosity but do not carry current. However, for the EIS measurements, ionomer does not need to be connected all the way through

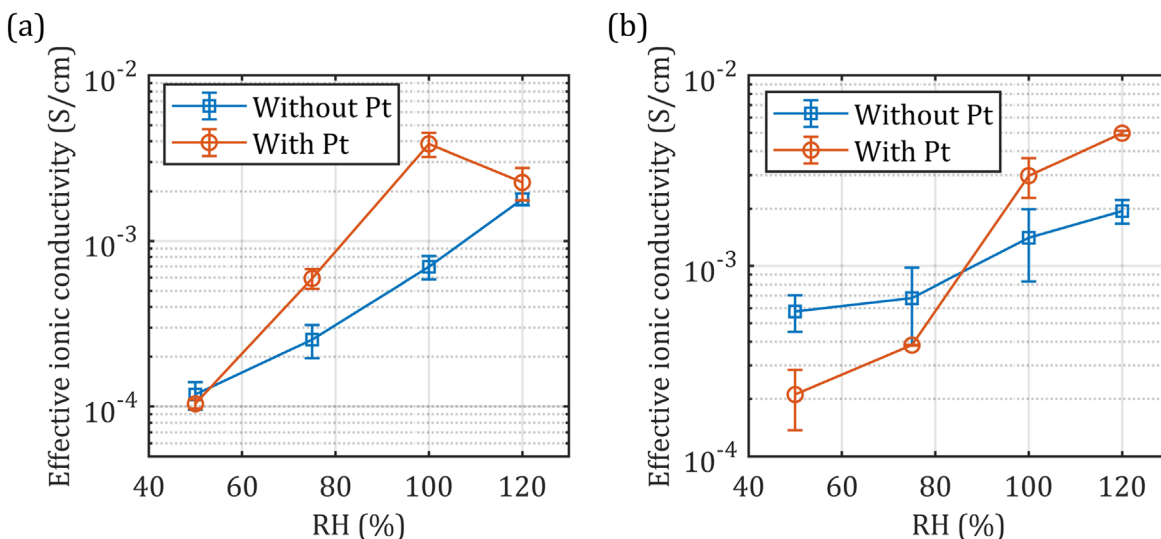


Figure 8. Effective ionic conductivity comparison between the PCL (without Pt) and Pt/C layer (with Pt) for (a) low I/C ratio ($I/C = 0.3$ for PCL and $I/C = 0.4$ for Pt/C) and (b) high I/C ratio of 1.2 for PCL and Pt/C in a RH range from 50% to 120%.

the PCL, if ionomer is in contact with membrane it will be proton current carrying. The ratio of the effective ionic conductivities between the EIS and AC HP increased with I/C ratio and decreased with RH. The highest ratio of effective ionic conductivities was found at 50% RH, which increased from 10 to 65 when I/C increased from 0.6 to 1.4. For RH of 120%, oversaturated conditions, where liquid water is expected to condense, the ratio between the two effective ionic conductivities differ by a ratio of 0.5 to 3. In fully saturated conditions ionomer connectivity will be high, and the two techniques should show similar results. However, in the low RH condition, more ionomer will be disconnected in both methods, as fewer water bridges exist between the ionomer clusters. Therefore, the difference in effective ionic conductivity and thus ionomer tortuosity are more pronounced at low RHs.

Mathematical modeling of the fuel cell has been conducted by using the effective ionic conductivities from EIS and AC HP methods for 50% and 75% RH. We observed the current density at 0.4 V increased from 0.74 A cm^{-2} to 1.08 A cm^{-2} at 50% RH when σ_{HP} and σ_{EIS} were used, respectively. Therefore, it is critical to input the correct effective ionic conductivity, which can be representative of the ion transport process in the catalyst layers, as the volume-average model approach relies on a single effective ionic conductivity through the whole catalyst layer.

Furthermore, we measured double layer capacitances and effective ionic conductivities with the EIS method for Pt/C catalyst layers with HSC and GrC supports and different I/C ratios for a RH range from 50 to 120% to emphasize the effect of I/C ratio, RH, and carbon support. Overall, with the same carbon support, the higher I/C ratio resulted in the higher double layer capacitance and effective ionic conductivity. Catalyst layer with the GrC support showed the highest effective ionic conductivity but lowest double layer capacity due to lower to no internal porosity, which results in a lower total surface area but better ionomer distribution. In contrast, Pt/C layer with the HSC support showed lower ionic conductivity but highest double layer capacity because the HSC support has high internal porosity, which resulted in worse ionomer distribution.

The effective ionic conductivities of the PCLs were compared to those of Pt/C with the same carbon support for the low I/C ratio (0.3–0.4) and high I/C ratio (1.2). We believe, the inks without Pt will have carbon agglomerations and for low I/C ratio these agglomerates will impact the ionic conductivity significantly, reducing it for the case of the PCLs. However, at higher I/C ratio, even if carbon agglomeration still occurs in the PCLs its impact on the ionomer distribution might not be as severe. Furthermore, Pt hydrophilicity and ionomer orientation will play a role in Pt/C

layers, where higher conductivity was observed for Pt/C for $I/C = 1.2$ at higher RH due to hydrophilic Pt retaining more water, helping proton transport.

Acknowledgments

This material is based upon work supported by the Department of Energy, Office of Energy Efficiency and Renewable Energy (EERE), under Award Number DE-EE0007650. SEM work was performed at the UC Irvine Materials Research Institute (IMRI). EDS work was performed at the IMRI as well, using instrumentation funded in part by the National Science Foundation Center for Chemistry at the Space-Time Limit (CHE-0802913).

ORCID

Yongzhen Qi <https://orcid.org/0000-0002-3996-2253>
 Ying Huang <https://orcid.org/0000-0002-8356-6194>
 Andrea Perego <https://orcid.org/0000-0002-3663-6890>
 Iryna V. Zenyuk <https://orcid.org/0000-0002-1612-0475>

References

1. Y. Manoharan, S. E. Hosseini, B. Butler, H. Alzahrani, B. T. F. Senior, T. Ashuri, and J. Krohn, *Appl. Sci.*, **9**, 2296 (2019).
2. J. Kast, R. Vijayagopal, J. J. Gangloff, and J. Marcinkoski, *Int. J. Hydrogen Energy*, **42**, 4508 (2017).
3. X. Liu, K. Reddi, A. Elgowainy, H. Lohse-Busch, M. Wang, and N. Rustagi, *Int. J. Hydrogen Energy*, **45**, 972 (2020).
4. A. Kongkanand and M. F. Mathias, *J. Phys. Chem. Lett.*, **7**, 1127 (2016).
5. T. R. Ralph and M. P. Hogarth, *Platinum Met. Rev.*, **46**, 117 (2002).
6. J. Huang, Z. Li, and J. Zhang, *Front. Energy*, **11**, 334 (2017).
7. A. Kusoglu and A. Z. Weber, *Chem. Rev.*, **117**, 987 (2017).
8. I. V. Zenyuk and S. Litster, *Electrochim. Acta*, **146**, 194 (2014).
9. A. Katzenberg, A. Chowdhury, M. Fang, A. Z. Weber, Y. Okamoto, A. Kusoglu, and M. A. Modestino, *J. Am. Chem. Soc.*, **142**, 3742 (2020).
10. Y. Furuya et al., *Effect of Ionomer Coverage on Pt-based Catalyst on ORR Activity*, Abstract #1522, 221st ECS Meeting, p. 234 (2011).
11. I. Rubinstein, *J. Electrochem. Soc.*, **133**, 729 (1986).
12. M. Eikerling and A. A. Kornyshev, *J. Electroanal. Chem.*, **475**, 107 (1999).
13. M. C. Lefebvre, R. B. Martin, and P. G. Pickup, *Electrochem. Solid-State Lett.*, **2**, 259 (1999).
14. Y. Liu, M. W. Murphy, D. R. Baker, W. Gu, C. Ji, J. Jorne, and H. A. Gasteiger, *J. Electrochem. Soc.*, **156**, B970 (2009).
15. Y. Liu, C. Ji, W. Gu, D. R. Baker, J. Jorne, and H. A. Gasteiger, *J. Electrochem. Soc.*, **157**, B1154 (2010).
16. R. Makharia, M. F. Mathias, and D. R. Baker, *J. Electrochem. Soc.*, **152**, A970 (2005).
17. R. Jiang, C. K. Mittelsteadt, and C. S. Gittleman, *J. Electrochem. Soc.*, **156**, B1440 (2009).
18. O. E. Barcia, E. D'Elia, I. Frateur, O. R. Mattos, N. Pébère, and B. Tribollet, *Electrochim. Acta*, **47**, 2109 (2002).

19. M. Obermaier, A. S. Bandarenka, and C. Lohri-Tymozhynsky, *Sci Rep.*, **8**, 1 (2018).
20. D. C. Sabarirajan, J. Liu, Y. Qi, A. Perego, A. Haug, and I. Zenyuk, *J. Electrochem. Soc.*, **167**, 084521 (2020).
21. H. Iden and A. Ohma, *J. Electroanal. Chem.*, **693**, 34 (2013).
22. J. Zhao, A. Ozden, S. Shahgaldi, I. E. Alaefour, X. Li, and F. Hamdullahpur, *Energy*, **150**, 69 (2018).
23. J. T. Gostick and A. Z. Weber, *Electrochim. Acta*, **179**, 137 (2015).
24. T. T. Nguyen, A. Demortière, B. Fleutot, B. Delobel, C. Delacourt, and S. J. Cooper, *NPJ Comput. Mater.*, **6** (2020).
25. A. Z. Weber et al., *J. Electrochem. Soc.*, **161**, F1254 (2014).
26. N. Ramaswamy, W. Gu, J. M. Ziegelbauer, and S. Kumaraguru, *J. Electrochem. Soc.*, **167**, 064515 (2020).
27. A. Haug et al., *DOE 2018 Annual Merit Review*, p. 239 (2018).